Molecular Physics, Vol. 104, No. 8, 20 April 2006, 1227–1237

Taylor & Francis
Taylor & Francis Group

Dynamics of fission and Coulomb explosion of multicharged large finite systems

Y. LEVY†, I. LAST and J. JORTNER*
Tel Aviv University, Israel

(*Received 16 June 2005; in final form 11 August 2005*)

This paper reports on studies of the fragmentation dynamics of multicharged $(A^+)_{55}$ Morse clusters, where the variation of the range of the Morse potential parameters induces cluster fission for a long-range potential and Coulomb explosion for a short-range potential. The multidimensional energy landscapes for these fragmentation processes were explored by constructing reduced coordinates utilizing the principal component analysis (PCA), which was previously applied for the energy landscapes and folding dynamics of biomolecules. The distance-matrix based PCA was applied to study the effects of the potential on the fragmentation dynamics and to explore the structural diversity of the fragmentation processes. The first principal coordinate (which captures 95% of the dynamic information content for each trajectory) constitutes an appropriate reaction coordinate for both fission and Coulomb explosion and was used to determine the temperature-dependent fragmentation rates. These obey the Arrhenius law, with the barrier for fission (0.36 eV) being higher than for Coulomb explosion (0.22 eV). Structural and energetic information on the radius of gyration and on the potential energy for small values of the reaction coordinate manifest considerably larger fluctuations for fission than for Coulomb explosion, indicating that in the former case the cluster shrinks and swells prior to dissociation. The joint projection of multiple trajectories for each fragmentation process allows for the description of the energy landscapes and fragmentation pathways in terms of two principal coordinates, which manifest a form of 'ski slopes'. Different collective coordinates describe the spatially isotropic Coulomb explosion and the spatially unisotropic fission.

1. Introduction

Cluster chemical physics explores the structure, energetics, function and dynamics of elemental, molecular and metallic clusters [1–8]. Electron-nuclear cluster dynamics laid the foundations for the elucidation of energy disposal, response to external electric, magnetic and laser fields, and chemical reactivity of large, finite systems [4–15]. Of considerable interest in the realm of cluster dynamics are fragmentation processes of multiply charged clusters, which are produced by clustering of ions [16–19], one-photon or multiphoton ionization [20–22], ionization by high-energy multicharged ions [23], and extreme multielectron ionization in ultraintense laser fields [24–35]. Ubiquitous fragmentation phenomena in multicharged, large finite systems driven by Coulomb (or pseudo-Coulomb [29]) forces involve clusters [16–21, 23, 24, 36–45], nuclei [46–49], droplets [50–52], and ultracold optical molasses [53].

The unique fragmentation patterns of multicharged finite systems do not have an analogue in the dynamics of the corresponding bulk matter [32, 34, 35]. In this context some interesting questions arise regarding the energetics and dynamics of dissociation:

(1) How does a finite system respond to a large excess charge or to an effective charge?
(2) What are the topography and topology of the multidimensional energy landscape that guide the system's shape, evolution, and fragmentation?
(3) What are the fragmentation channels and under what conditions are they realized?
(4) What is the interplay between fission, i.e. instability towards dissociation, of the finite system into two (or a small number of) fragments and

*Corresponding author. Email: jortner@chemsg1.tau.ac.il
† Present address: Department of Physics, 6230 Urey Hall, University of California at San Diego, 9500 Gilman Drive, La Jolla, California 92093-0371.

Molecular Physics
ISSN 0026–8976 print/ISSN 1362–3028 online © 2006 Taylor & Francis
http://www.tandf.co.uk/journals
DOI: 10.1080/00268970500525630

Coulomb explosion into a large number $\sim n$ (where n is the number of constituents) of ionic species?

In a previous study [54, 55], we reported on the fragmentation of highly charged $(A^+)_n$ ($n = 55$, 135, 321) Morse clusters. These multicharged clusters were investigated by molecular dynamics simulations by varying the range of the pair potential and of the Rayleigh fissibility parameter X, which is defined by the ratio E(Coulomb)/2E(surface). The constant energy molecular dynamics simulations were performed on a time scale of up to 1 ns with the multicharged cluster being subjected at $t = 0$ to a final temperature of $T = 500$–10^4 K. The fragmentation process results in the fragments of cluster ions A_k^{k+} ($1 \leq k < n$) of sizes n_k with $\sum_k kn_k = n$. For the long-range Morse potential, the clusters fragment into a small number of large, multicharged clusters, which contain the majority of the ions, and thus correspond to cluster fission. The fragmentation pattern is qualitatively different for the short-range Morse potential and involves a large number of small ionic fragments and, accordingly, corresponds to Coulomb explosion. The fragmentation patterns via either fission or Coulomb explosion are practically temperature independent. The fission process is spatially unisotropic, with the deformation of the parent multicharged cluster along a one-axis elongation forming two large clusters. The Coulomb explosion process, on the other hand, is spatially isotropic with the small ionic fragments expanding radially. The fission and the Coulomb explosion process also differ in the kinetic energies of the fragments. For fission, the kinetic energies and the internal energies of the large fragments are high, with the total kinetic energy being comparable to the total inner energy. For Coulomb explosion the major kinetic energy of the fragments is considerably larger than the inner energy.

In this paper, we address the dynamics of fission and of Coulomb explosion by exploring the energy landscapes for these processes. This is illustrated for a Morse cluster composed of 55 ions, each with a single positive charge. A comparison between the two processes is achieved by applying Principal Component Analysis (PCA) [56–60] to several trajectories of both processes at different temperatures. PCA was originally introduced to describe the energy landscapes and folding dynamics of biophysical systems, e.g. polypeptides and proteins [57–65]. We shall show that PCA constitutes a useful tool for describing the dimensionality of the dynamics and of the potential energy landscapes that underlie cluster fission and Coulomb explosion processes. The principal coordinates for fission and for Coulomb explosion capture the essential information of their dynamics and are accordingly appropriate reaction coordinates. Projecting the multidimensional dynamics onto the principal coordinates enables one to explore the kinetics and structural properties of the fragmentation of highly charged clusters.

2. Methods

2.1. *Molecular dynamics simulations*

We applied classical (constant energy) molecular dynamics simulations to study the dynamics of Coulomb explosion and fission processes of a multicharged $(A^+)_{55}$ cluster. The mass of each A^+ ion is 100 amu, its charge is $q = 1$, and the total cluster charge is $Z = 55$. The interionic pair potential $U(R)$ consists of an attractive Morse potential and of Coulomb repulsion,

$$U(R) = DG(G - 2) + Bq^2/R \tag{1}$$

where

$$G = \exp[-\alpha(R - R_e)] \tag{2}$$

D is the dissociation energy, α is a range parameter, R_e is the Morse potential equilibrium distance, and $B = 14.385\,\text{eV/Å}$. Two sets of Morse potential parameters were used: (i) A short-range Morse potential with $D = 4.5$ eV, $\alpha = 3\,\text{Å}^{-1}$, and $R_e = 3$ Å ($\alpha R_e = 9$, so that the interaction between non-neighboring atoms is negligibly small); (ii) A long-range Morse potential, with $D = 6.5$ eV, $\alpha = 1\,\text{Å}^{-1}$, and $R_e = 2$ Å ($\alpha R_e = 2$, so that the contribution of interactions between non-neighbouring atoms is of significance). For each set of Morse potential parameters 15 trajectories were collected in the temperature range 3000–8000 K (three simulations at each temperature, labelled in figure 1). The trajectories obtained at each temperature were used to study the fragmentation kinetics and to sample different regions of the potential energy surface of the fragmentation under the short- and long-range potentials. The initial $t = 0$ nuclear configuration of the multicharged cluster is presented in the icosohedral geometry of the low temperature ($T = 10$ K) cluster, with a thermal, Maxwell distribution of the velocities of the atoms, which was obtained after an equilibration time of 1000 fs at the low temperature. Thermal excitation was achieved by a temperature jump to a temperature T. This thermal excitation by a 'temperature jump' involves complete intramolecular vibrational relaxation within the multicharged ionic cluster. The molecular dynamics simulations were performed using the 5-value Nordsieck predictor–corrector algorithm. We used different seed numbers for generating the

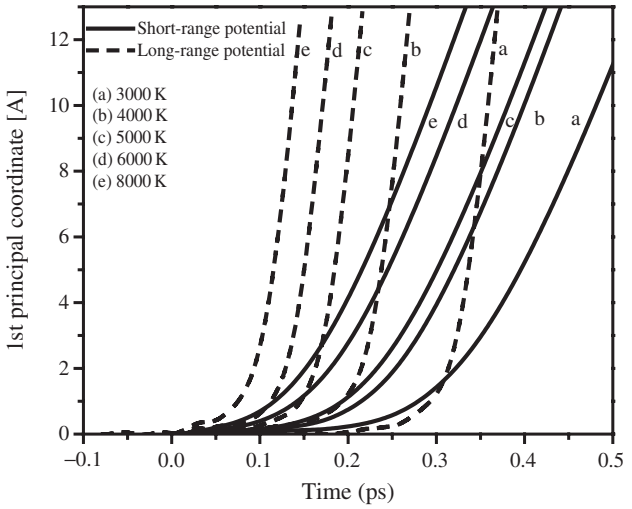

Figure 1. Time evolution of the first principal coordinate for the cluster fragmentation under short-range (——) and long-range (– – – –) potentials for representative trajectories simulated at temperatures in the range 3000–8000 K. Temperatures labelled on curves.

initial velocity distribution, and a propagation time step of 0.02 fs, with the structure being sampled for every 20 fs. The system's dynamics can be described as dissociation of the cluster into ionic fragments followed by their translational motion while keeping their sizes constant. Here, we are mainly interested in the early dynamics stages of the charged clusters, which involve the fragmentation mechanism of the parent clusters under short-range and long-range Morse potentials, rather than the escape dynamics of the fragments, where the fragments' translational dynamics constitutes the main dynamics after dissociation. Accordingly, only configurations with a maximal radius smaller than a specific cutoff value were considered. For the $(A^+)_{55}$ cluster simulated with a short-range and a long-range Morse potential, these cutoffs were taken as 4 and 8 times the initial radius of the equilibrated icosohedral cluster, respectively. The cutoff values were chosen to ensure that the dynamics on the two potential energy landscapes will be represented on similar reaction coordinates.

To study the fragmentation pattern of the charged cluster with short-range and long-range potentials, two time-dependent structural measures were selected. The first is the radius of gyration $Rg(t)$, which reflects the compactness of the cluster ions,

$$Rg(t) = \sqrt{\frac{1}{n}\sum_{i=1}^{n}(r_i(t) - r_{CM}(t))^2} \qquad (3)$$

$r_i(t)$ is the set of Cartesian coordinates of the ith ion at time t, n is the number of ions, and r_{CM} is the position of the centre of mass. The second measure is the maximal ellipsoid volume occupied by the cluster ions. While both structural measures may capture dissociation of the cluster and the spatial dynamics of their fragments, the radius of gyration cannot distinguish between isotropically and unistropically spatial dissociation while, in principle, the maximal ellipsoid volume can provide this information.

2.2. *Principal component analysis*

In general, $(3n–6)$ coordinates are required to describe the dynamics of the cluster. However, since both the fission and the Coulomb explosion of a multicharged $(A^+)_n$ cluster are not spatially homogeneous but take place along specific directions of the fragment motions (in 1D space and in 3D space for the fission and for the Coulomb explosion, respectively) not all the coordinates are important. As a result a much smaller number of coordinates is sufficient to capture the dynamical characteristics of these processes. Reducing the effective dimensionality of these systems can be achieved by using the PCA, which is based on the principle that the Cartesian coordinates are not necessarily the best ones to describe dynamics of complex systems. It is possible to reveal some new properties of the dynamics by describing it in a different set of coordinates [56, 57]. The PCA reduces the effective dimensionality by choosing orthogonal components, so that the variance in the original data is well described. Accordingly, the relations of similarity/dissimilarity among the original data can be well approximated in the reduced description. Projecting the original multidimensional data onto an optimal low-dimensional subspace allows for the visualization of trajectories and for the mapping of energy landscapes [56, 58–60, 66].

PCA methods have been extensively applied to study the dynamics of molecules and, in particular, biological macromolecules such as proteins [57–65]. The PCA is often applied on the $m \times m$ covariance matrix,

$$C_{ij} = \left\langle (x_i - \langle x_i \rangle)(x_j - \langle x_j \rangle) \right\rangle \qquad (4)$$

where $m = 3n$, with n being the number of atoms. The averaging is over the instantaneous structures sampled during the ith period of simulation and x_i is an atomic coordinate. The covariant matrix-based PCA concentrates on the collective motion of the atoms and was successfully applied to find functionally relevant motions of proteins [57, 59–65]. Another approach is to apply the PCA on the $N \times N$

distance-matrix, where N is the number of sampled conformations. The distance-matrix based PCA was used to compare the conformational space of analogous molecules and thus provides a visualization and a quantitative measure for the shifting and shrinking (or increasing) of the conformational space as a result of structural constraints [67], point mutations [68, 69], and the chemical environment [60]. Recently, the distance-matrix based PCA was used to study the effects of dimerization on the flexibility of a protein [70, 71]. However, it should be pointed out that, because usually $N > m$, the distance-matrix-based PCA is computationally more expensive than the more common covariance-matrix-based PCA due to matrix diagonalization. In this study, we apply the distance-matrix-based PCA to study the structural diversity of the fragmentation of multicharged clusters and to explore the effects of the potential on the fragmentation dynamics.

The PCA starts from $N \times m$ data matrix M, which holds the m coordinates defining N configurations in an m-dimensional space. That is, each matrix element M_{ij} is equal to q_{ij}, the jth coordinate of the ith configuration. PCA operates on the square $N \times N$, MM^T matrix, reflecting the relationships between the configurations (the snapshots along a trajectory). The elements of this matrix, also known as the distance matrix Δ, are the d_{ij} distances between two configurations i and j of a given chemical system. In this study, the d_{ij} distance is measured by the RMS deviation in Cartesian coordinates between the i and j configurations and is defined as the minimum of the functional

$$d_{ij} = \sqrt{\frac{1}{n}\sum_{k=1}^{n}\left|\mathrm{r}_k^{(i)} - \mathrm{r}_k^{(j)}\right|^2} \tag{5}$$

where $k = 1{-}n$ is an index over the ions, and $\mathrm{r}_k^{(i)}$, $\mathrm{r}_k^{(j)}$ are the Cartesian coordinates of the kth ion in the i and j configurations, respectively. The minimum value d_{ij} of equation (5) is obtained by an optimal superposition of the two configurations. Since the d_{ij} distances can also be obtained from the $N \times N$ matrix A of latent roots (eigenvectors), one can use this matrix for the projection, defining $\mathrm{A}_{ij} = -1/2d_{ij}^2$ and $\mathrm{A}_{ii} = 0$ (for i, $j = 1, 2, \ldots, n$). To ensure that the A matrix has a zero root (and thus guarantee that it corresponds to a real configuration) it is 'centred', so that the sum of every row and the sum of every column of A is zero. This centring, which does not alter the d_{ij} distances, is defined by

$$A_{ij}^{*} = A_{ij} - \langle A_{ij}\rangle_i - \langle A_{ij}\rangle_j + 2\langle A_{ij}\rangle_{ij} \tag{6}$$

where $\langle\cdot\rangle_k$ is the mean over all the specific indices $k = i, j, ij$. The centred matrix A^* is diagonalized using standard matrix algebra to obtain the latent eigenvectors and the diagonal matrix of eigenvalues. The resulting (normalized) eigenvalues give the percentage of the projection of the original distribution on the new coordinate set, and the eigenvectors (scaled by their corresponding eigenvalues) give the new coordinates of the original points in the new axes set [56, 59]. Following the PCA procedure, each new axis k is associated with a normalized eigenvalue, λ_k, that represents the relative weight of that axis in reproducing the original data. An axis with a high value of λ_k is significant for the projection, whereas axes with small values of λ_k are insignificant. By sorting the new axes according to their λ_k weight it is possible to select a small subset of effective coordinates that captures most of the configurational relationships of the original high-dimensional space. It was found that in polypeptide systems the effective dimensionality of conformational spaces is significantly smaller than the dimensionality of the full spaces, with only a few principal axes contributing to the projection. In fact, in many cases a projection quality of 70–90% can be achieved for a subspace spanned only by three effective coordinates [67, 69, 72].

The PCA is useful for the reduction of the dynamic dimensionality of complex systems, as well as for the comparison between different sets of trajectories in the same system, which are obtained from different conditions. For example, the dynamics along two trajectories of a $(\mathrm{A}^+)_n$ multicharged cluster simulated for the same or for a different potential can be obtained. When configurations of two sets of trajectories, a and b, of the same molecular system are to be compared with each other, the 'cross' distance matrix, $\Delta_{a,b}$, must be calculated in addition to the two self-distance matrices, Δ_a and Δ_b. The elements of the rectangular 'cross' matrix are the distances between all configurations of set a and of set b. Thus, to obtain a joint projection of sets a and b within the same molecular system, the PCA is applied to the combined **D** matrix,

$$\mathbf{D} = \begin{pmatrix} \Delta_a & \Delta_{a,b} \\ 0 & \Delta_b \end{pmatrix} \tag{7}$$

where Δ_a and Δ_b are the upper diagonal 'self'-distance matrices and $\Delta_{a,b}$ is the rectangular 'cross' distance matrix. The size of the joint **D** matrix is $(N + N') \times (N + N')$, with N configurations in set a and N' configurations in set b. Equation (7) is easily extended to any arbitrary number of configuration sets.

In this study, we applied the PCA to project the multidimensional cluster fragmentation dynamics on a subspace, and thus explore the complex dynamics of the cluster fragmentation. More specifically, the dynamics along a single trajectory was studied by applying the PCA for configurations collected along each trajectory. It should be noted that, because the fragmentation mode is determined in the early stage of the dynamics, which is followed by diffusion motion, a single reaction coordinate is expected to be sufficient to characterize the dynamics. In addition, all the structures collected along the 15 trajectories obtained from the simulations with the short-range potential, as well as from those obtained with the long-range potential, were projected using the PCA in order to compare the fragmentation dynamics along each trajectory and to characterize the energy landscape. Finally, all structures obtained from all simulations (i.e. both with the short-range and with the long-range potential) were jointly projected using the PCA to reflect the difference in the dynamics induced by the two potentials.

3. Results

The fragmentation process of a multicharged $(A^+)_{55}$ cluster was explored by applying PCA to the analysis of sets of trajectories simulated on the energy landscapes, which are determined by the potentials, equations (1) and (2), with the parameters specified in section 2.1. The dynamics of the cluster prior to and after fragmentation is different. While the dynamics before and during fragmentation is dominated by deformation of the cluster due to fluctuations of the positions of the cluster ions, motion of the fragments characterizes the post-fragmentation dynamics. Post-fragmentation dynamics is obviously more extensive than pre-fragmentation dynamics. Using PCA, the multidimensional dynamics can be viewed by projecting each dissociation trajectory onto a subspace defined by several collective coordinates. In this study, we focus mainly on exploring the pre-fragmentation dynamics, however, the simple translational dynamics of the fragments after dissociation can assist in characterizing the collective reaction coordinate. Accordingly, a single collective coordinate may be sufficient to describe the dynamics. This collective coordinate will serve as the reaction coordinate, which captures the fragmentation of the cluster and the motion of the fragments.

Figure 1 portrays the time evolution of the first principal coordinate (the principal axis with the largest eigenvalue) obtained when projecting representative trajectories simulated at five different temperatures. It should be noted that the reaction coordinate might be different among the trajectories because the fragmentation pattern can be affected by the temperature and by the initial velocity distribution. The reaction coordinate was independently obtained for each trajectory by applying the PCA and was found to have a large ($>95\%$) normalized eigenvalue, reflecting the high weight of that axis in reproducing the original data. For the sake of a simpler comparison, all the principal coordinates were shifted to zero at $t=0$. The propagations of the dissociation reactions along the principal coordinates indicate that they are good reaction coordinates for the characterization of cluster fragmentation. The dissociation rate was estimated by the time τ required to achieve 5 Å on the first principal coordinate of each of the three trajectories simulated at each temperature. Some variations exist in the dissociation rates of these trios of simulations, indicating the complexity of their energy landscape. Yet, the averaged dissociation rates from the trios of trajectories at different temperatures can be used to obtain an estimate of the activation barrier for cluster fragmentation. More extensive sampling has to be performed to study the detailed kinetics. Figure 2 shows the temperature dependence of the fragmentation rates and indicates that the dissociation rate obeys the Arrhenius law. The $x=\log(1/\tau)$ and $y=1/T$ axes in figure 2 correspond to the logarithm of the dissociation rate and the inverse of the temperature, respectively. The activation barrier for dissociation under

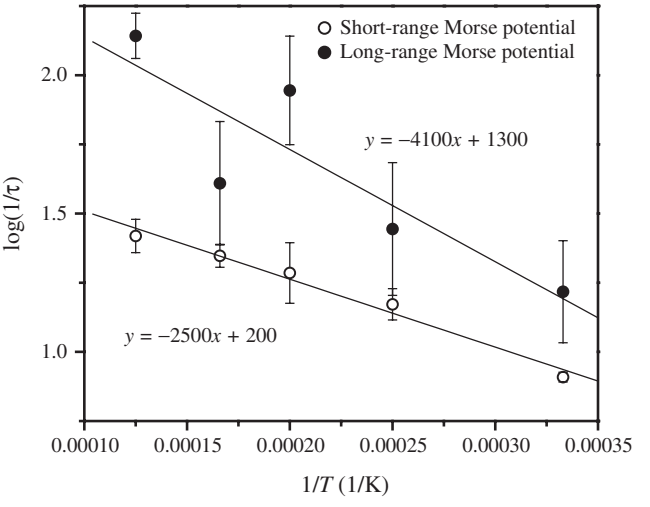

Figure 2. Arrhenius analysis of the fragmentation rate as a function of temperature. The $x=\log(1/\tau)$ and $y=1/T$ axes correspond to the logarithm of the averaged dissociation rate (estimated by the time τ required to achieve 5 Å on the first principal coordinate of each of the three trajectories simulated at a given temperature) and the inverse of the temperature, respectively.

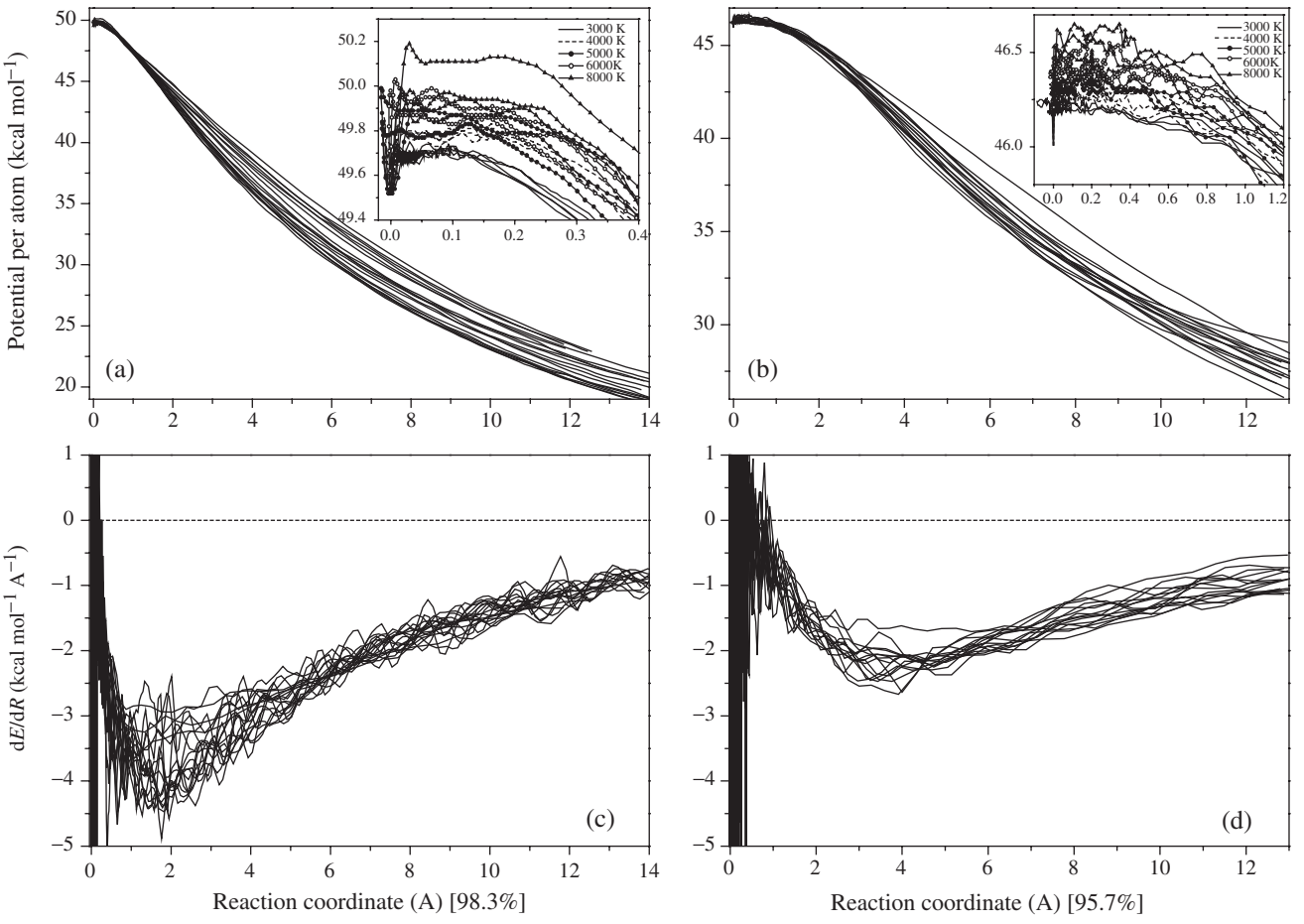

Figure 3. The potential energy decays along the reaction coordinates for all the trajectories calculated under (a) short-range and (b) long-rang Morse potentials. For each trajectory, the reaction coordinate is the principal axis with the largest eigenvalue and captures about 95% of the dynamics information. The slopes of potential energy profiles (dE/dR), which were obtained under short-range and long-range Morse potentials, are shown in figure 3(c) and 3(d), respectively. For a clear presentation, in all the figures the initial icosohedral structure was shifted to the origin.

long-range and short-range Morse potentials are 0.36 and 0.22 eV, respectively, showing that the barrier for fission is about 75% higher than that for Coulomb explosion.

Figures 3(a) and 3(b) show the decrease of the potential energy along the reaction coordinates for the short-range and for the long-range potentials, respectively. The insets indicate that regions of the potential energy surfaces with higher potential energy are sampled at higher temperatures. While the potential energy decay curves, which were obtained for short-range and for long-range Morse potentials, are similar at high values of the reaction coordinate, they are different at the early stage of the fragmentation dynamics. The simulated potential energy of the cluster at short distances ($\sim$1 Å) manifests larger fluctuations for the long-range potential, considerably exceeding those for the short-range potential (insets to figures 3a and 3b). The latter observation suggests that for an energy landscape generated by long-range interactions, the cluster undergoes swelling, lengthening and shrinking prior to dissociation. For reaction coordinates smaller than 5 Å the potential energy slope, dE/dR, is larger with the short-range potential than with the long-range potential (figures 3(c) and 3(d)). However, at the later stages of the dynamics (i.e. above 5 Å along the reaction coordinates), the slope of the potential energy along the reaction coordinate is very similar for both potentials. This indicates that in that region the long-range interactions are dominated by the Coulomb repulsion and the cluster fragments move independently with both short-range and long-range potentials.

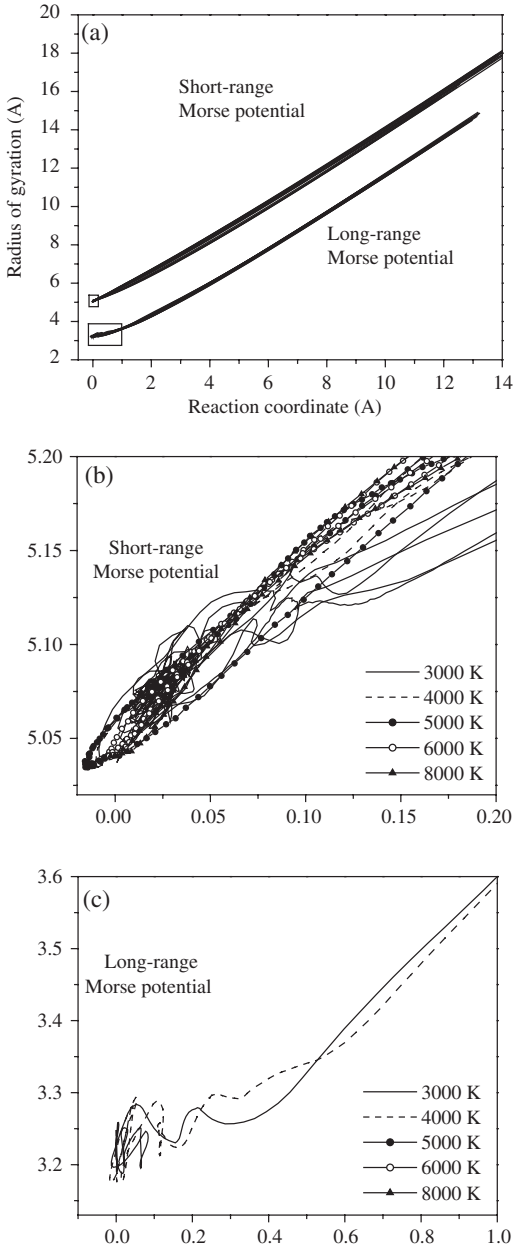

Figure 4. (a) Time-dependent radius of gyration, $Rg(t)$, along the trajectories simulated with short-range and long-range Morse potentials. Figures (b) and (c) present the radius of gyration at the fragmentation of the cluster, before the cluster swells as a result of the fragmentation dynamics (they correspond to the region of the Radius of gyration and of the Reaction coordinates marked by rectangles in (a)). The enhanced fluctuations of the fragmentation obtained with the long-range Morse potential suggest that the dynamics is more complicated and might be characterized by swelling and shrinking.

The time-dependent radii of gyration, $Rg(t)$, along the trajectories collected under short-range and long-range Morse potentials are shown in figure 4. The increase of the radius of gyration for both potentials reflects on dissociation induced by the repulsive electrostatic forces. Figures 4(b) and 4(c) describe the radius of gyration prior to fragmentation and indicate that, while the $Rg(t)$ profiles are very similar at high values of the reaction coordinate, they reveal a different pattern at low values of this coordinate. The oscillations in the radius of gyration of the cluster calculated for the long-range potential are much more pronounced than those observed for the short-range potential and they are larger for higher temperatures. $Rg(t)$ along the trajectories simulated with the long-range potential shows marked fluctuations of up to 0.8 Å of the reaction coordinate. On the other hand, the fluctuations are minor and persist for about 0.1 Å of the reaction coordinate for the trajectories simulated with the short-range potential. The different characteristics of $Rg(t)$ before and during fragmentation in the two Morse potentials suggest that the cluster experiences shrinking and swelling prior to dissociation due to the long-range interactions, while with short-range interactions the cluster dissociates almost without the involvement of breathing motions.

To complement the fragmentation dynamics with structural properties, we calculated the time dependence of the maximal ellipsoid volume of the ions from the fragmenting clusters. The maximal ellipsoid volume increases smoothly along the reaction coordinate that describes the dissociation processes for both Morse potentials. However, for the short-range Morse potential the increase of the maximum ellipsoid volume is considerably larger (figure 5). The latter observation indicates that the dynamics under the short-range potential is more isotropic than that under the long-range potential. This conclusion is supported by dynamic information from the simulations.

Figure 6 presents several snapshots, which illustrate the different patterns of the fragmentation of the charged $(A^+)_{55}$ clusters under the short-range and under the long-range potentials. The cluster dissociation should be described as a fission process when it is induced by a long-range potential, and as a Coulomb explosion when it is induced by a short-range potential. The fission and the Coulomb explosion reactions have different characteristics. The fission reaction occurs mainly along one dimension, however, the dynamics of the Coulomb explosion is nearly spatially isotropic. Moreover, cluster fission results in fewer fragments than Coulomb explosion, which ends up with many small fragments.

PCA was further applied for a joint description of all the trajectories obtained for each potential. While the projection of a single trajectory onto a principal axis enables the study of its dynamic characteristics along the reaction coordinate, the joint projection of multiple

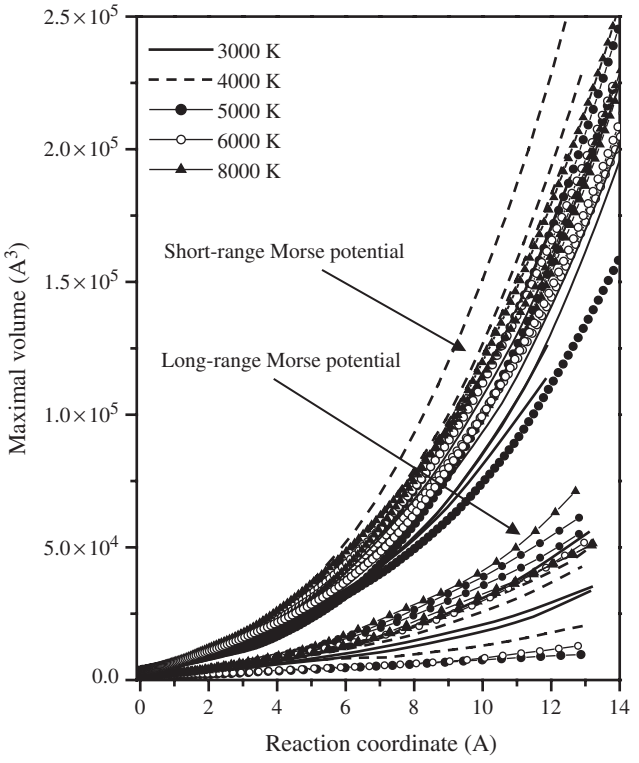

Figure 5. Time dependence of the maximal ellipsoid volume of the ions constituting the cluster. Note the sharper increase in the ellipsoid volume in the case of the short-range potential, which may indicate more isotropic dynamics.

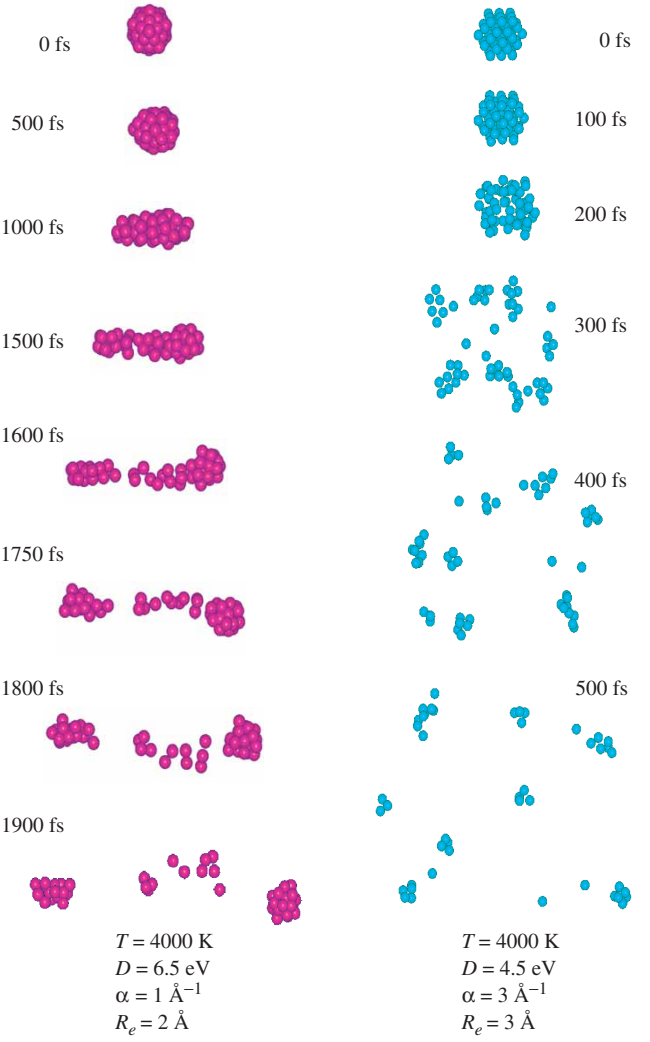

Figure 6. Several snapshots illustrating the different patterns of fragmentation of the charged $(A^+)_{55}$ cluster under short-range (right) and long-range (left) potentials. The cluster dissociation corresponds to a fission process, which takes place mainly along one dimension (left), and to a spatially isotropic Coulomb explosion in three dimensions (left). Moreover, the cluster fission results in a few ionic fragments, while the Coulomb explosion results in many small fragments.

trajectories onto the same principal axis provides a useful tool to explore the effects of the energy landscape on the dynamics and to characterize the number of possible reaction pathways. This approach was applied to study the potential energy surfaces for fission and for Coulomb explosion. Projecting all the trajectories on the same principal axes can be achieved only after measuring the RMS deviations, equation (5), between all pairs of configurations in each trajectory, as well as the RMS deviation between any configurations for each trajectory and all configurations from the other trajectories, equation (7). The joint projection of the 15 trajectories of the dissociation of the $(A^+)_{55}$ cluster under short-range and long-range potentials are shown in figures 7(a) and 7(b), respectively. The first and second principal coordinates of the joint projection of all the short-range trajectories capture 47 and 11% of the dynamics, respectively. The observation that the first principal coordinate captures only 47% of the dynamics of the cluster dissociation when jointly projected (in comparison to 98% when projected individually) illustrates the diversity of Coulomb explosion pathways among the different trajectories. Even lower values (20 and 18% for the first and second principal coordinates, respectively) were obtained for the joint projection of the trajectories simulated with the long-range potential, reflecting widely different pathways during the fission process. The decay of the potential energy landscapes of the cluster during dissociation is similar for both fission and for Coulomb explosion (figures 7(a) and 7(b)) and can be described as 'ski slopes'. For a given fragmentation mode, the projected trajectories do not overlap, indicating that the fragmentation pathways differ in their trajectories for both Coulomb explosion and for fission. Accordingly, while the cluster undergoes

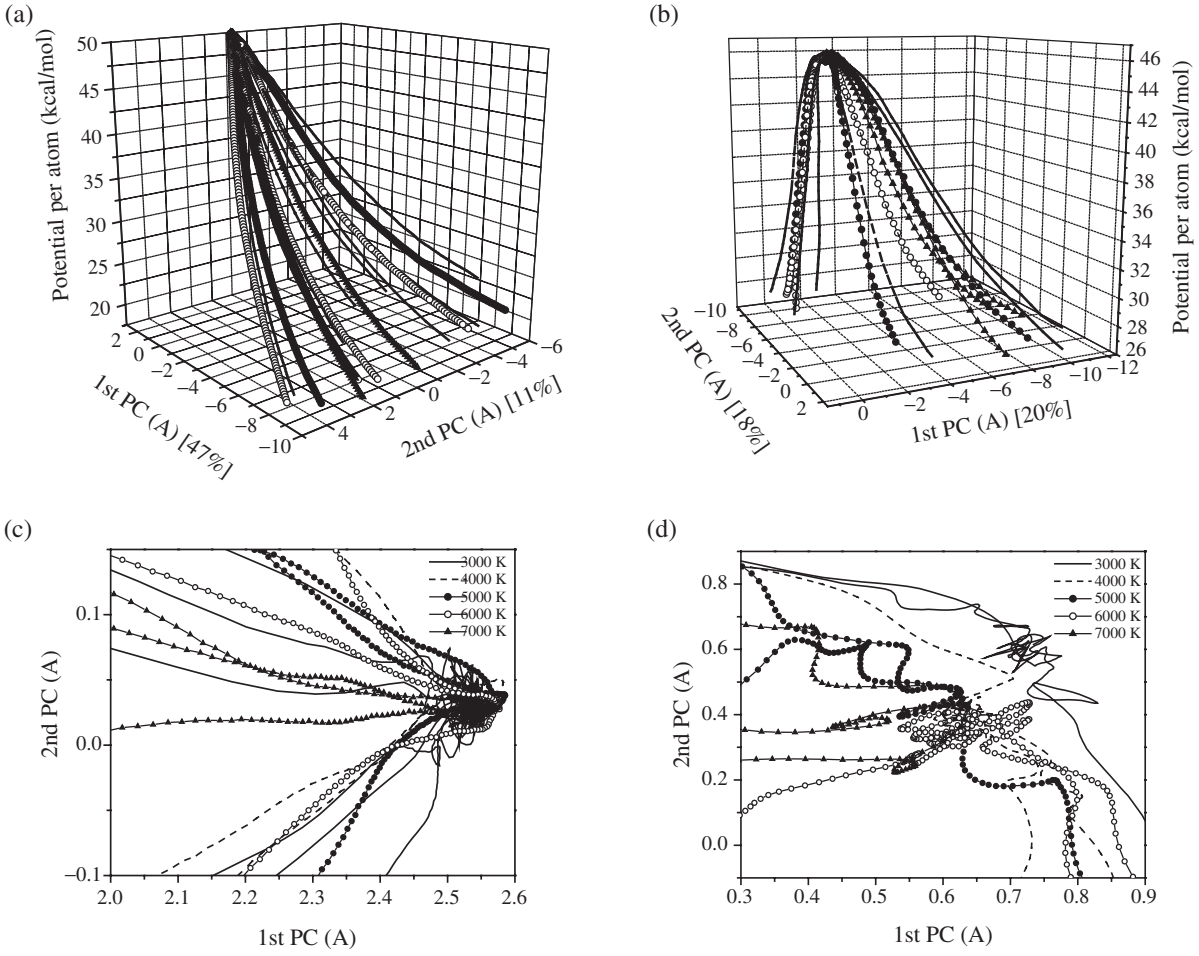

Figure 7. Potential energy decay landscapes of the cluster ions during their dissociation along two principal axes. The principal axes were obtained by joint projection of all the trajectories simulated with short-range (a) and (c) and long-range (b) and (d) Morse potentials. Figures (c) and (d) show the projected trajectories at the early stage of the cluster dynamics.

Coulomb explosion under the short-range Morse potential, the number of small fragments, their size, and composition might be different from one trajectory to another. Similar features characterize the cluster fission. The trajectories simulated at the same temperatures sometimes do not show the same fragmentation pattern. The oscillations in the trajectories in the two-dimensional principal coordinate spaces are observed at the early stage of fragmentation for cluster fission (figure 7(d)), compared with the smooth patterns of these trajectories for Coulomb explosion (figure 7(c)). This observation concurs with the fluctuations observed in the time dependence of the radius of gyration (figure 4), and indicates that the dynamics of fission is more complex than that of Coulomb explosion. While cluster fission and its fragmentation into a small number of fragments involves cluster swelling, lengthening, and shrinking, cluster explosion into a large number of small clusters is dynamically simpler.

To establish the different dimensionality of the fragmentation processes, PCA was applied to construct the joint projection of the trajectories for both fission and for Coulomb explosion on the same two-principal axis. Figure 8 shows that such a joint projection of the trajectories reflects on different patterns of dissociation for fission and for Coulomb explosion. While all the trajectories for Coulomb explosion, as well as all the trajectories for fission, are essentially represented by a single principal axis, there is a qualitative distinction between the two sets of trajectories. The Coulomb explosion dynamics is dominated by the first principal axis (which captures 55% of the dynamic information). On the other hand, the fission dynamics is dominated by the second principal axis (which captures only 7% of the dynamic information). The relatively low eigenvalues obtained when jointly projecting the short-range and the long-range Morse potential trajectories is indicative of limited reproduction of the original

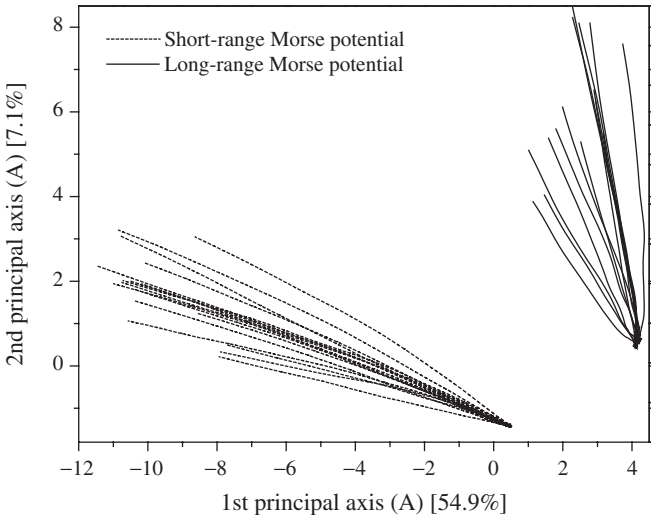

Figure 8. Joint projection of all the fission and Coulomb explosion trajectories on the same two principal axes. The first and second principal axes capture 54 and 8% of the dynamic characteristics, respectively.

high-dimensional space. We would like to emphasize that because of this limitation, the principal coordinates were used as reaction coordinates to infer on fission and on Coulomb explosion, kinetics were obtained by applying PCA to each single trajectory. However, although a principal coordinate capturing 7% of the dynamic information is not very significant, it is still meaningful because it manifests the spatially heterogeneous dynamics of the different trajectories. Furthermore, the joint projection of all the trajectories illustrates that different collective coordinates describe the spatially isotropic Coulomb explosion and the spatially unisotropic fission.

4. Conclusions

We studied the structural and dynamic features of the fragmentation of multicharged Morse clusters during fission and during Coulomb explosion. The multidimensional energy landscapes for these processes were explored by applying the PCA method to reduce the effective dimensionality and for finding the principal coordinates that capture the essential dynamic information. The first principal coordinate was found to be an appropriate reaction coordinate for both fission and Coulomb explosion processes and was used to estimate the fragmentation rates of the cluster at different temperatures. The dissociation rates obey the Arrhenius law and indicate that the barrier for fission is about 50% higher than that for Coulomb explosion. In addition, the collective coordinates serve to study the fragmentation pathways. The fission and Coulomb explosion processes have distinct dynamical properties. The fission process is spatially unistropic and involves breathing motions of swelling, lengthening and shrinking of the cluster prior to complete dissociation, which is characterized by the motion of the fragments. The Coulomb explosion process exhibits a simpler dynamic behaviour, being spatially isotropic with the small ionic fragments expanding radially. The present study manifests unifying features of chemical dynamics in large finite systems, with PCA providing a useful scheme for both isomerization (and folding) dynamics of biomolecules [56–60], and 'reactive' fragmentation dynamics of clusters.

Acknowledgements

This research was supported by the Deutsche Forschungsgemeinschaft (DFG) SFB 450 on 'Analysis and Control of Ultrafast Photoinduced Reactions' and by the Binational German–Israeli James Franck programme on laser–matter interaction.

References

[1] R. Kubo, J. Phys. (Paris) **38,** 270 (1977).
[2] J. Friedel, J. Phys. (Paris) **38,** 1 (1977).
[3] E. W. Schlag, R. Weinkauf, and R. E. Miller, Chem. Phys. **239,** 1 (1988).
[4] T. Kondow, K. Kaya, and A. Terasaki, *Structure and Dynamics of Clusters* (Universal Academy Press, Tokyo, 1996).
[5] C. Yannouleas and U. Landman, Eur. Phys. J. D **16,** 9 (2001).

[6] J. Jellinek, *Theory of Atomic and Molecular Clusters* (Springer, Berlin, 1999).
[7] H. Haberland, *Clusters of Atoms and Molecules* (Springer, Berlin, 1994).
[8] J. Jortner, Z. Phys. D **24,** 247 (1992).
[9] J. Jortner, Zeit. Physik. Chemie-Int. J. Res. Phys. Chem. Chem. Phys. **184,** 283 (1994).
[10] J. Jortner, J. De Chimie, Phys. Physico-Chimie Biol. **92,** 205 (1995).
[11] A. P. Alivisatos, Science **271,** 933 (1996).
[12] B. von. Issendorff and O. Cheshnovsky, Ann. Rev. Phys. Chem. **56,** 549 (2005).
[13] V. Bonacic-Koutecky and R. Mitric, Chem. Rev. **105,** 11 (2005).
[14] J. Jortner and C. N. R. Rao, Pure Appl. Chem. **74,** 1491 (2002).
[15] S. Khanna, A. W. Castleman, *Quantum Phenomena in Clusters and Nanostructures* (Springer, Berlin, 2002).
[16] P. Scheier and T. D. Märk, Chem. Phys. Lett. **136,** 423 (1987).
[17] M. Lezius and T. D. Märk, Chem. Phys. Lett. **155,** 496 (1989).
[18] S. Sugano, A. Tamura, and Y. Ishii, Zeit. Physik D-Atoms Mol. Clusters **12,** 213 (1989).
[19] M. Lezius, P. Scheier, A. Stamatovic, and T. D. Märk, J. Chem. Phys. **91,** 3240 (1989).
[20] N. Gotts, P. Lethbridge, and A. Stace, J. Chem. Phys. **96,** 408 (1992).
[21] H. J. Krappe, Zeit. Physik D-Atoms Mol. Clusters **23,** 269 (1992).
[22] N. Saito, K. Koyama, and M. Tanimoto, Chem. Phys. Lett. **300,** 262 (1999).
[23] C. Guet, X. Biquard, P. Blaise, *et al*., Zeit. Physik D-Atoms Mol. Clusters **40,** 317 (1997).
[24] T. Ditmire, T. Donnelly, A. M. Rubenchik, R. W. Falcone, and M. D. Perry, Phys. Rev. A **64,** 3379 (1996).
[25] T. Ditmire, J. W. G. Tisch, E. Springate, M. B. Mason, N. Hay, J. P. Marangos, and M. H. R. Hutchinson, Phys. Rev. Lett. **78,** 2732 (1997).
[26] M. H. R. Hutchinson, T. Ditmire, E. Springate, J. W. G. Tisch, Y. L. Shao, M. B. Mason, N. Hay, and J. P. Marangos, Philos. Trans. R. Soc. London Series a-Math. Phys. Eng. Sci. **356,** 297 (1998).
[27] T. Ditmire, E. Springate, and J. W. G. Tisch, Phys. Rev. A **57,** 369 (1998).
[28] E. Springate, N. Hay, J. W. G. Tisch, M. B. Mason, T. Ditmire, M. H. R. Hutchinson, and J. P. Marangos, Phys. Rev. A **57,** 369 (1998).
[29] J. Kou, N. Nakashima, S. Sakabe, S. Kawato, H. Veyama, T. Urano, T. Kuge, Y. Izawa, and Y. Kato, Chem. Phys. Lett. **289,** 334 (1998).
[30] M. Lezius, S. Dobosz, D. Normand, *et al*., Phys. Rev. Lett. **80,** 261 (1998).
[31] I. Last and J. Jortner, Phys. Rev. A **62,** 03201 (2000).
[32] I. Last and J. Jortner, J. Chem. Phys. **120,** 1336 (2004).
[33] I. Last and J. Jortner, J. Chem. Phys. **121,** 3030 (2004).
[34] I. Last and J. Jortner, J. Chem. Phys. **121,** 8329 (2004).
[35] N. Bohr and J. A. Wheeler, Phys. Rev. **56,** 426 (1939).
[36] D. Kreisle, O. Echt, M. Knapp, *et al*., Phys. Rev. Lett. **56,** 1551 (1986).
[37] A. J. Stace, P. G. Lethbridge, and J. E. Upham, J. Phys. Chem. **93,** 333 (1989).
[38] C. Brechignac, P. Cahuzac, J. Leygnier, *et al*., J. Chem. Phys. **90,** 1492 (1989).
[39] I. Katakuse, H. Ito, and T. Ichihara, Int. J. Mass Spectrometry Ion Process. **97,** 47 (1990).
[40] C. Brechignac, P. Cahuzac, F. Carlier, and M. de Frutos, Phys. Rev. Lett. **64,** 2893 (1990).
[41] W. A. Saunders and N. Dam, Zeit. Phys. D-Atoms Mol. Clusters **20,** 111 (1991).
[42] W. A. Saunders, Phys. Rev. A **46,** 7028 (1992).
[43] C. Brechignac, P. Cahuzac, F. Carlier, and M. de Frutos, Phys. Rev. B **49,** 2825 (1994).
[44] A. Goldberg, I. Last, and T. F. George, J. Chem. Phys. **100,** 8277 (1994).
[45] U. Naher, S. Bjornholm, S. Frauendorf, *et al*., Phys. Rep.-Rev. Sect. Phys. Lett. **285,** 245 (1997).
[46] L. Meitner and O. R. Frisch, Nature **143,** 239 (1939).
[47] S. Frenker and N. Metropolis, Phys. Rev. **72,** 914 (1947).
[48] P. Moller, D. G. Madland, A. J. Sierk, and A. Iwamoto, Nature **409,** 785 (2001).
[49] P. Heyde, *Basic Ideas and Concepts in Nuclear Physics* (Institute of Physics Publishing, Bristol, 1994).
[50] D. C. Taflin, T. L. Ward, and E. J. Davis, Langmuir **5,** 376 (1989).
[51] J. F. Widman, C. L. Arrdhal, and E. J. Davis, Aerosol Sci. Technol. **27,** 636 (1979).
[52] D. Duft, T. Achtzehn, R. Muller, and T. Leisner, Nature **421,** 128 (2003).
[53] L. Pruvost, I. Serre, H. T. Duong, and J. Jortner, Phys. Rev. A **61,** 053408 (2000).
[54] I. Last, Y. Levy, and J. Jortner, Proc. Natl Acad. Sci. USA **99,** 9107 (2002).
[55] I. Last, Y. Levy, and J. Jortner, J. Chem. Phys. **123,** 154031 (2005).
[56] O. M. Becker, J. Comput. Chem. **19,** 1255 (1998).
[57] A. Kitao and N. Go, Curr. Opin. Struct. Biol. **9,** 164 (1999).
[58] O. M. Becker, J. Mol. Struct. (THEOCHEM) **398,** 507 (1997).
[59] Y. Levy and O. M. Becker, J. Chem. Phys. **114,** 993 (2001).
[60] Y. Levy, J. Jortner, and O. M. Becker, Proc. Natl. Acad. Sci. USA **98,** 2188 (2001).
[61] A. Kitao and N. Go, J. Comput. Chem. **12,** 359 (1991).
[62] A. E. Garcia, Phys. Rev. Lett. **68,** 2696 (1992).
[63] A. E. Garcia and J. G. Harman, Protein Sci. **5,** 62 (1996).
[64] A. Amadei, A. B. M. Linssen, and H. J. C. Berendsen, Proteins Struct. Funct. Genet. **17,** 412 (1993).
[65] S. Hayward and N. Go, Ann. Rev. Phys. Chem. **46,** 223 (1995).
[66] Y. Levy and O. M. Becker, Phys. Rev. Lett. **81,** 1126 (1998).
[67] O. M. Becker, Y. Levy, and O. Ravitz, J. Phys. Chem. B **104,** 2123 (2000).
[68] Y. Levy, E. Hanan, B. Solomon, and O. Becker, Proteins Struc. Funct. Genet. **45,** 382 (2001).
[69] Y. Levy and O. M. Becker, Proteins **47,** 458 (2002).
[70] Y. Levy and A. Caflisch, J. Phys. Chem. B **107,** 3068 (2003).
[71] Y. Levy, G. A. Papoian, J. N. Onuchic, *et al*., Israel J. Chem. **44,** 281 (2004).
[72] Y. Levy, J. Jortner, and O. Becker, J. Chem. Phys. **115,** 10533 (2001).